On the Application of Line Distributed Singularities for Fast Non-Empirical Prediction of Tonal Rotor Noise

Andrea Franco[1,2,3], Michael Mößner[2], Roland Ewert[2] and Jan W. Delfs[2]

[1] *Cluster of Excellence SE²A –Sustainable and Energy-Efficient Aviation, Technische Universität Braunschweig, Germany*

[2] *Institute of Aerodynamics and Flow Technology, Department of Technical Acoustics, German Aerospace Center (DLR), Lilienthalplatz 7, 38108 Braunschweig, Germany*

[3] *, Email: andrea.franco@dlr.de*

Introduction

In the last decade, the increasing demand for international mobility has seen an equivalent growth in air transportation, therefore increasing its environmental impact. As a consequence, the necessary cuts in environmental pollution require sustainable aviation designs concepts that would need, among the targets to achieve, significant noise emission reductions. Sustainable approaches in aircraft design that include the integration of unconventional propulsion concepts on the airframe have been progressively proposed and adopted as viable solutions [1], therefore requiring reliable noise emissions' predictions tools to evaluate the feasibility of such proposals with regards to their environmental impact, directly aiding aircraft manufacturers during the design stage of an aircraft. For this purpose, in [2] a fast and physical-principles-based rotor noise model was introduced, together with suitable adapted perturbation equations to represent current and possibly newly arising noise sources mechanisms. The rotor noise model is based on rotating point or line sources that represent loading noise in terms of equivalent body forces. The perturbation equations presented are derived from the Linearised Euler Equations (LEE), which are split into two separate perturbation equation systems related to the acoustic and vorticity mode. The resulting system of equations, named APE+VCE, includes the Acoustic Perturbation Equations (APE) as main acoustic governing equation, and the Vortical Convection Equation as the equation describing the convection of the hydrodynamic component of the velocity perturbations. The approach proposed was applied in a Computational Aeroacoustics (CAA) framework in the time domain, and implemented in the unstructured quadrature-free experimental Discontinuous Galerkin (DG) CAA solver DISCO++ of DLR. The APE+VCE equations' system is solved on a tetrahedral grid, where, for each tetrahedron, the solution is represented with a third-order polynomial. Time integration is performed with a fourth-order Runge-Kutta method. In this contribution, the benefit of modelling rotor blades by means of line-distributed sources is investigated. An analysis of the effect on the sound field due to the possibility of defining the location of the distributed loads on straight or curved lines is considered and compared with results obtained from corresponding closed form solutions of the wave equation in an unbounded domain. In the sections APE+VCE System Of Equations, Line-Distributed Source Model, and Closed Form Solution, the governing perturbation equations are briefly presented, together with the line-distributed rotor model and the closed-form pressure field solution used, derived from the superposition of multiple rotating point sources. In the section Results of Simulated Test Cases, the comparison of the solutions obtained from the CAA simulations and the closed-form pressure field formula is presented and analyzed for the selected test cases, and concluding, future developments are indicated.

Line-Distributed Source Model

The CAA simulations performed in this work are based on the approach described in [2]. In this method, the modelled rotor sources are obtained as a Gaussian regularisation of three-dimensionally line-distributed input forces, rotating uniformly around the rotor axis. The line-distributed source values are specified as obtained from either simplified Blade Element Momentum (BEM) theories, actuator disk Reynolds Averaged Navier Stokes (RANS) solutions, or unsteady RANS simulations of geometrically-resolved rotors. The sources are prescribed to the high-order points of the computational grid based on a local cylindrical coordinate system centered at the rotor hub being modelled. Starting from an initial location $\boldsymbol{X_{init}} = (r_{init}, \phi_{init}, x_{init})^T$, the time dependent source location described by the circumferential coordinate ϕ_{time} is determined from the source's revolutions per second n prescribed in input.

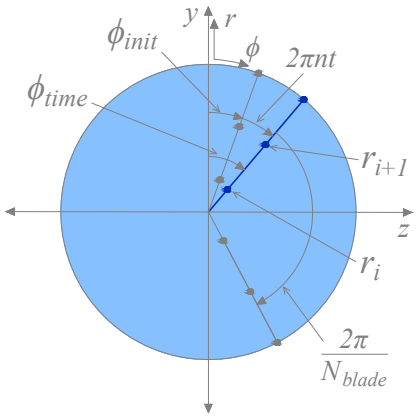

Figure 1: Rotor cylindrical coordinate system for a line-distributed source.

If the modelled rotor includes multiple blades N_{blade}, the initial location of each line source is defined assuming an equi-spaced circumferential offset $2\pi/N_{blade}$ applied to ϕ_{init}. Figure (1) presents the geometrical quantities of interest for the line-distributed source model. The regularisation of sources is performed in two steps. Since the radial distribution is known from the input values prescribed, in a first step the value at a given radial grid location r_{Grid} is obtained by linear interpolation of the load values included in the range $[r_i, r_{i+1}]$, resulting in $\boldsymbol{f_{Interp}} = (f_{Interp,r}, f_{Interp,\phi}, f_{Interp,x})^T$. This first step reduces the necessary dimensions over which regularising is required, therefore in the second step the regularisation of the load values is obtained by convolution of $\boldsymbol{f_{Interp}}$ with the Gaussian kernel $K(\phi_{Src}, x_{Src}, \phi_{Grid}, x_{Grid})$, defined as:

$$K(\phi_{Src}, x_{Src}, \phi_{Grid}, x_{Grid}) = \left(\frac{ln(2)}{\pi}\right)\frac{1}{\varepsilon^2}\exp\left(\frac{-ln(2)d^2}{\varepsilon^2}\right) / \operatorname{erf}\left(\frac{\pi\sqrt{(ln(2))}r_{Src}}{\varepsilon}\right) \quad (1)$$

in which

$$d = \sqrt{r_{Src}^2(\phi_{Src} - \phi_{Grid})^2 + (x_{Src} - x_{Grid})^2} \quad (2)$$

represents the distance measured on a cylindrical surface defined at a radius r_{Src}, where ϕ_{Src} is the line source azimuthal location, ϕ_{Grid} the grid point azimuthal coordinate, x_{Src} the line source axial location, and x_{Grid} the grid point axial coordinate. The half-width at half-maximum of the Gaussian kernel is represented by ε. Details on the definition of Eq. (1) and Eq. (2) are included in [2]. The source values regularised with Eq. (1) are described as the sum of a steady mean and a fluctuating component, where only the fluctuating component is of interest for the perturbation equations considered. The perturbed regularised force value is therefore determined as $\boldsymbol{S'} = \boldsymbol{S} - \boldsymbol{S_{mean}}$, where the mean value $\boldsymbol{S_{mean}}$ is computed as the average source value over a single rotor revolution, which in the case of constant rotational speed can be alternatively expressed as a spatial integral over a ring of given radius. The resulting fluctuating sources' values $\boldsymbol{S'}$ are then assigned to the appropriate point of the DG discretization.

APE+VCE System Of Equations

The fluctuating source values are prescribed to the APE+VCE system of perturbation equations, introduced in [2]. The APE+VCE equations' system was formulated to tackle simplified as well as more complex configurations that investigate propulsion installation-related noise, and it reads as:

$$\frac{\partial p'}{\partial t} + c_0^2\nabla\cdot\left(\boldsymbol{u_0}\frac{p'}{c_0^2} + \rho_0\boldsymbol{u^a}\right) = -c_0^2\nabla\cdot(\rho_0\boldsymbol{u^r}) + c_0^2\dot{\theta'} \quad (3)$$

$$\frac{\partial \boldsymbol{u^a}}{\partial t} + \nabla(\boldsymbol{u^a}\cdot\boldsymbol{u_0}) + \nabla\left(\frac{p'}{\rho_0}\right) = \boldsymbol{0} \quad (4)$$

$$\frac{\partial(\rho_0\boldsymbol{u^r})}{\partial t} + \nabla\cdot(\rho_0\boldsymbol{u_0}\boldsymbol{u^r}) + \rho_0(\boldsymbol{u^r}\cdot\nabla)\boldsymbol{u_0} = -\rho_0\boldsymbol{\omega_0}\times\boldsymbol{u^a} + \boldsymbol{f'} \quad (5)$$

where ρ, $\boldsymbol{u}$, p, and t are the density, velocity, pressure, and time, respectively, with subscript 0 indicating mean flow quantities and primed symbols indicating perturbation quantities. c_0 represents the speed of sound and $\boldsymbol{\omega_0}$ the vorticity vector, both computed from the mean flow. The fluctuating velocity $\boldsymbol{u^a}$ describes the potential (acoustic) component of the perturbed velocity of the LEE, while $\boldsymbol{u^r}$ is the non-acoustic component of the LEE velocity, which includes the solenoidal field of the LEE. The fluctuating source terms of the LEE can be assigned to $\dot{\theta'}$ for air displacement type of sources, and to $\boldsymbol{f'}$ for externally prescribed fluctuating forces.

Closed Form Solution

The results obtained from the CAA simulations are compared with a suitable closed form solution of the wave equation. The option considered involves the superposition of solutions of the wave equation for rotating point forces in an unbounded domain, following the procedure described in [3]. Equation (6) describes the solution considered in this context:

$$p'_{f_p}(\boldsymbol{x},t) = \frac{1}{4\pi}\left\{\frac{\frac{\partial \boldsymbol{f_p}}{\partial\tau}\cdot\boldsymbol{e_R} + (\boldsymbol{f_p}\cdot\boldsymbol{e_R})\frac{\partial \boldsymbol{M_q}}{\partial\tau}\cdot\boldsymbol{e_R}(1-M_{qR})^{-1}}{a_\infty R_i(1-M_{qR})^2}\right\} + \frac{1}{4\pi}\left\{\frac{-\boldsymbol{f_p}\cdot\boldsymbol{M_q} + (1-\boldsymbol{M_q}^2)\boldsymbol{f_p}\cdot\boldsymbol{e_R}(1-M_{qR})^{-1}}{R_i^2(1-M_{qR})^2}\right\} \quad (6)$$

$\boldsymbol{M_q}$ is the Mach number of the moving source, $\boldsymbol{x}$ the observer position, $\boldsymbol{y(\tau)}$ the point source position dependent on the retarded time τ, $R_i = |\boldsymbol{R_i}| = |\boldsymbol{x} - \boldsymbol{y(\tau)}|$ the distance between source and observer, $\boldsymbol{e_R} = \boldsymbol{R_i}/R_i$ the unit distance vector between source and observer, $\boldsymbol{M_{qR}} = \boldsymbol{M_q}\cdot\boldsymbol{e_R}$ the momentary Mach number component in the direction of the observer, and a_∞ the speed of sound. In the presence of a uniform flow, the distance R_i changes as $R_i = |\boldsymbol{R_i}| = |\boldsymbol{x} - \boldsymbol{y(\tau)} - \boldsymbol{U_\infty}(\tau - t)|$, and the Mach number changes as well as $\boldsymbol{M_q} = \boldsymbol{M_q} + \boldsymbol{U_\infty}$, where $\boldsymbol{U_\infty}$ represents the free stream velocity vector.

Results of Simulated Test Cases

The test cases identified include a single propeller blade modelled as a straight and a curved line source, where in both cases the same load values are prescribed, corresponding to a realistic thrust distribution adapted from existing surface load data of a wing-tip mounted propeller, and scaled to generate a qualitative relevant acoustic response. Fig. (2) presents the distribution for the test cases considered. The curved line source values locations have been prescribed along the curve shown in Fig. (3), defining in the line source model multiple three dimensional linear segments. In the computational grid, the regularized line source is resolved inside a cylindrical refinement region that ensures an appropriate representation of the propagating vortex. The rotating straight line source is defined in a y-z plane, and both curved and straight line sources are centered at $(x, y, z) = (-0.4, -0.15, 0.0)$.

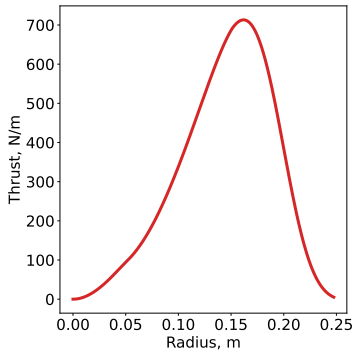

Figure 2: Thrust input distribution.

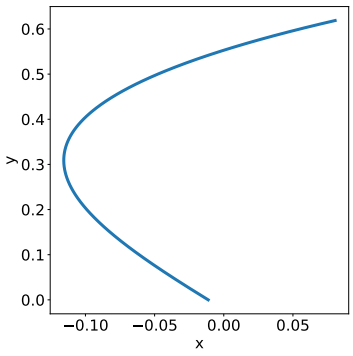

Figure 3: Curved line source definition.

The size of the tetrahedral cells in the farfield is specified to resolve the first ten harmonics, and in the refinement region it is reduced to 1/10 of the farfield tetrahedral edge length. A ratio of $\varepsilon/\Delta x_{Ref} = 2$ was selected for the Gaussian regularized sources. The boundary condition on the outer surfaces that enclose the computational domain is of the non-reflecting type, formulated based on an upwind flux vector splitting approach, with prescribed null incoming eigenmodes. Approximately five complete revolutions of the line source are simulated. All the results obtained from closed form pressure field solutions and from CAA simulations are presented in terms of Sound Pressure Level (SPL), displaying the 1st, 3rd, and 5th frequency mode of the fluctuating pressure signals, captured on the x-y coordinate plane at a distance of 4R from the origin of the line source local coordinate system. Table (1) summarises the simulation input parameters. The computational domain is sketched in Fig. (4).

Table 1: Simulations Input Parameters

Input Parameter	Value
Free-stream Mach nr. M_∞	0.17
n	218.77 s^{-1}
Propeller Blade Length R	0.2032 m
Farf. Tetra Cell Size Δx_{Far}	0.3224
Refin. Tetra Cell Size Δx_{Ref}	0.03224
Number of Time Steps	200,000
Time Step Size	0.0001

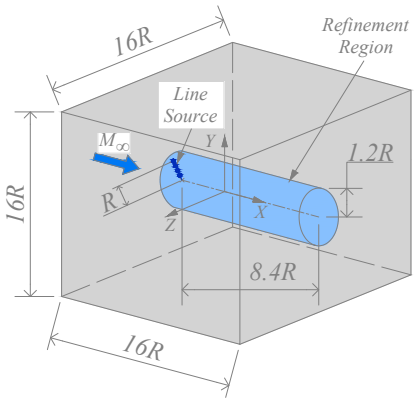

Figure 4: Computational domain for the selected test cases.

A qualitative inspection of the results for both the straight and curved line source test cases shows how the current implementation successfully describes the change in curvature of the regularized curved line source. Fig. (5) and Fig. (6) present the results of the test cases as pressure fluctuations contour plots, with Q-Criterion iso-surfaces superimposed, computed from $\boldsymbol{u^r}$.

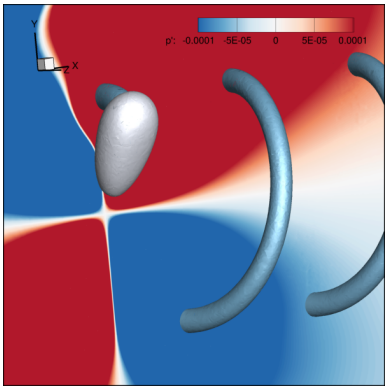

Figure 5: Contour plot of p' for the straight line test case, with Q-Criterion superimposed

Quadrupole-type pressure fluctuation patterns are identifiable, and the ring vortex pattern, generated due to the rotation of the line-distributed source, changes its cross-sectional shape in the curved line source test case, as expected.

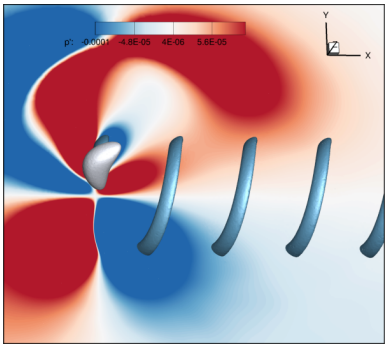

Figure 6: Contour plot of p' for the curved line test case, with Q-Criterion superimposed

Figure (7), Fig. (8) and Fig. (9) show the results of the test cases considered for the 1st, 3rd, and 5th frequency mode of the fluctuating pressure signals. The solution of each test case is displayed alongside its corresponding closed form solution obtained from Eq. (6).

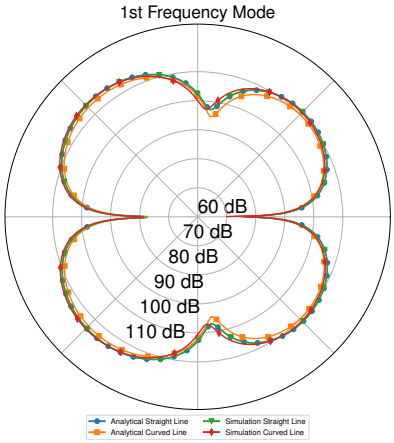

Figure 7: SPL (dB) comparison for the 1st frequency mode

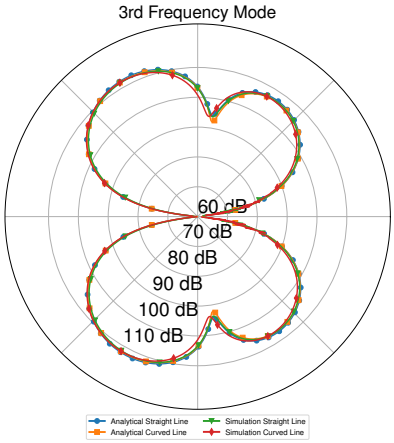

Figure 8: SPL (dB) comparison for the 3rd frequency mode

For the 1st mode, the results of the CAA simulation of a straight line source show a very good agreement with the corresponding solution from Eq. (6). For the curved line source CAA simulation, a slight overall overprediction of the SPL can be detected, which appears more pronounced in the 1st and 4th quadrant of the polar plot. The 3rd mode results of the curved line source test case show a slight underprediction of SPL when compared with the corresponding closed form solution, whereas for the straight line test case a close correspondence with its analytical counterpart is maintained. The CAA solutions analysed in terms of the 5th mode present a general slight underprediction of the results, more noticeable for the curved line source test case. A close inspection of only the results of the CAA simulations shows a distinct change in directivities' pattern, noticeable in the region between the first and second quadrant of the polar plot. Overall, the correct implementation of the line source model for the straight and curved line source test cases

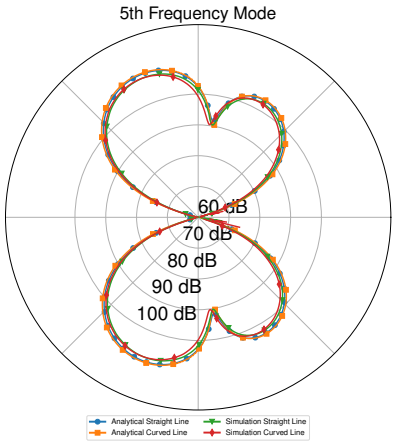

Figure 9: SPL (dB) comparison for the 5th frequency mode

is verified, as can be seen from the very close correspondence of the directivities considered, and only minor differences in SPL levels are seen in the curved line source validation.

Conclusion

In a previous contribution, a new approach for the prediction of propulsion installation-related noise was developed in a CAA framework, including the newly proposed APE+VCE system of perturbation equations, in combination with regularized line-distributed sources that replace the physical rotor blades. In this work, the line sources' implementation was verified for a single straight and curved line source configuration. The results obtained verify the correct realization of the model implemented. As future development, a comparison against available experimental data will be performed, to investigate the need for a possible alternative curved line source model formulation.

Acknowledgments

We would like to acknowledge the funding by the Deutsche Forschungsgemeinschaft (DFG, German Research Foundation) under Germany's Excellence Strategy –EXC 2163/1-Sustainable and Energy Efficient Aviation –Project-ID 390881007.

References

[1] Gohardani, A. S., Doulgeris, G., and Singh, R., "Challenges of future aircraft propulsion: A review of distributed propulsion technology and its potential application for the all electric commercial aircraft," Progress in Aerospace Sciences, Vol. 47, No.5, 2011, pp. 369, 391. https://doi.org/10.1016/j.paerosci.2010.09.001

[2] Franco, A., Ewert, R., Mößner, M., and Delfs, J. W., "Towards a Fast Non-Empiric Source Model for Installed Rotor Noise," AIAA Aviation 2021 Forum. https://doi.org/10.2514/6.2021-2240

[3] J.W. Delfs, Basics of Aeroacoustics. Lecture notes, (2019). http://www.dlr.de/as/desktopdefault.aspx/tabid-191/401_read-22566/skript_GrundlagenAeroakustikWS.pdf